Construction of a Biological Tissue Model Based on a Single-Cell Model: A Computer Simulation of Metabolic Heterogeneity in the Liver Lobule

Hiroshi Ohno**,†
Keio University

Yasuhiro Naito*,**,†,‡
Keio University

Hiromu Nakajima§
Osaka Medical Center
   for Cancer and
   Cardiovascular Diseases

Masaru Tomita**,†,‡
Keio University

Abstract An enormous body of information has been obtained by molecular and cellular biology in the last half century. However, even these powerful approaches are not adequate when it comes to higher-level biological structures, such as tissues, organs, and individual organisms, because of the complexities involved. Thus, accumulation of data at the higher levels supports and broadens the context for that obtained on the molecular and cellular levels. Under such auspices, an attempt to elucidate mesoscopic and macroscopic subjects based on plentiful nanoscopic and microscopic data is of great potential value. On the other hand, fully realistic simulation is impracticable because of the extensive cost entailed and enormous amount of data required. Abstraction and modeling that balance the dual requirements of prediction accuracy and manageable calculation cost are of great importance for systems biology. We have constructed an ammonia metabolism model of the hepatic lobule, a histological component of the liver, based on a single-hepatocyte model that consists of the biochemical kinetics of enzymes and transporters. To bring the calculation cost within reason, the porto-central axis, which is an elemental structure of the lobule, is defined as the systems biological unit of the liver, and is accordingly modeled. A model including both histological structure and position-specific gene expression of major enzymes largely represents the physiological dynamics of the hepatic lobule in nature. In addition, heterogeneous gene expression is suggested to have evolved to optimize the energy efficiency of ammonia detoxification at the macroscopic level, implying that approaches like this may elucidate how properties at the molecular and cellular levels, such as regulated gene expression, modify higher-level phenomena of multicellular tissue, organs, and organisms.

---

  * Contact author.

** Institute for Advanced Biosciences, Keio University, 14-1 Baba-cho, Tsuruoka, 997-0035, Japan. E-mail: n02139ho@sfc.keio.ac.jp

  † Bioinformatics Program, Graduate School of Media and Governance, Keio University, 5322 Endo, Fujisawa, 252-8520, Japan.

  ‡ Department of Environmental Information, Keio University, 5322 Endo, Fujisawa, 252-8520, Japan. E-mail: ynaito@sfc.keio.ac.jp (Y.N.); mt@sfc.keio.ac.jp (M.T.)

  § Clinical Laboratory, Osaka Medical Center for Cancer and Cardiovascular Diseases, 1-3-3 Nakamichi, Higashinariku, Osaka, 537-0025, Japan. E-mail: nakajima-hi@mc.pref.osaka.jp

1 Introduction

Systems biology is intended to elucidate the dynamics of the biological cell based on a compendium of data carried out by what might be called the "ome" and the "omics" sciences, such as the genome and genomics, the proteome and proteomics, or the metabolome and metabolomics [21, 26]. Meanwhile, biological life, which it is hoped will come to be understood, is rarely restricted to a single cell, or unicellular organism. The human being is a representative multicellular organism, consisting of approximately 60 trillion cells, and undoubtedly the subject that we would like to investigate most intensively. At present, the greater part of the data that support systems biology is information at the molecular and cellular (nanoscopic and microscopic) levels. While the explosive development of molecular and cellular biology has yielded both copious and precise information at the subcellular level, biology for higher-level (mesoscopic and macroscopic) structures has lagged far behind. Anatomy and histology represent an organism in a hierarchical classification scheme, namely of tissues, organs, and individual, going from the microscopic to macroscopic. The store of knowledge built up at each level of the hierarchy is at present disproportionate. The knowledge accumulated in the last decade at higher levels than the cell is undoubtedly less than that at the cellular and subcellular levels. A major constraint is the currently limited technology, which for the tissue or organ level presents greater difficulties in all aspects of sample preparation, cultivation, and measurement than required for the single-cell level.

Hitherto, nanoscopic and microscopic mathematical models for the life sciences have been isolated from mesoscopic and macroscopic ones in most cases, while mesoscopic and macroscopic entities inevitably consist of macroscopic entities. Here we report an effort to expand the knowledge of cellular, subcellular, and molecular levels to higher levels such as tissues and organs through biological simulation, which is one of the main contributions of systems biology. We are aware that such a bottom-up approach is not always appropriate; for instance, a description of solid-body motion with quantum mechanics is almost always pointless. However, given the overwhelming shortage of quantitative information at the mesoscopic and macroscopic levels, a serious effort to elucidate higher-level behaviors of life based on the abundant molecular and cellular data collected is of value whatever the difficulty entailed. To construct a tissue or organ model based on a single-cell model, simple aggregation of the cell model into a higher-level model is essentially inadequate. Not only organs of complicated structure such as the heart and brain, but those of comparatively simple structure such as the liver and kidney, are impossible to model by simple multiplication of single cells, because each tissue or organ has its own intrinsic and exquisitely specific structure. The spatiotemporal position of the cells in the tissue or organ structure influences the behavior of each cell, and the total of the cellular behaviors naturally affects the behaviors of the higher structures—the tissue, organ, or organism—in turn. Therefore, how to effectively assemble the single-cell model(s), namely, how to represent the mesoscopic and macroscopic structure, is critically important for the modeling of tissues and/or organs.

For this study the rodent liver was selected as the subject of modeling because of (1) its comparatively simple histological structure among mammalian tissues and organs [37], and (2) the availability of data from previous investigations, including a great deal of kinetic data. The liver consists of a huge structure consisting of repetitions of a fundamentally simple structural unit, the hepatic lobule. The entire liver looks the like a bunch of grapes, in which the portal tracts (influx vessels) and the central vein (efflux vessel) supply each bunch (Figure 1A). The portal tracts are a bundle of small branches of the hepatic portal vein, which carries the absorbed food products directly from the gut to the liver, and the hepatic artery, which supplies oxygen to support liver metabolism. The central veins are confluent and form the hepatic vein. The hepatic lobule is roughly hexagonal in sectional configuration and is centered on a central vein. The portal tracts are positioned at the corners of the hexagon. The blood from the portal vein and hepatic artery branches in the portal tracts flows to a central vein (Figure 1B, C). The overwhelmingly predominant component of the liver is the parenchymal liver cell, called the hepatocyte. The hepatocytes form branching
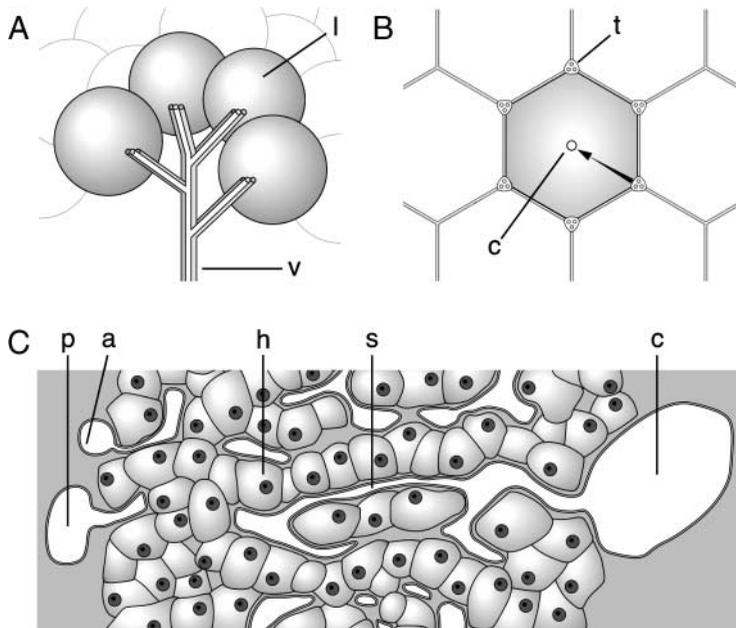
Figure 1. Schematic drawings of the connection of the hepatic lobules in the liver (A), hexagonal shape of a hepatic structure in section (B), and the porto-central axis (C). l, a hepatic lobule; v, influx and efflux vessels consist of terminal branches of the portal vein, hepatic artery, and hepatic vein; t, periportal tracts; c, central vein; p, terminal portal vein; a, terminal hepatic artery; s, sinusoid; h, hepatocyte. The arrow indicates the direction of sinusoidal blood flow.

cords of cells between capillary vessels, which are known as sinusoids in the hepatic lobule. Blood flow into the sinusoids comes from terminal branches of the portal tracts, bringing nutrient-rich blood from the portal vein and oxygen-rich blood from the hepatic artery. Blood from the portal vein and the hepatic artery passes through the sinusoids, where it comes into intimate contact with the hepatocytes for the exchange of nutrients and metabolic products. The blood then flows into branches of the hepatic vein and thence into the inferior vena cava. Therefore, the liver can be described histologically as a rough hierarchy of the hepatocyte (cell), the hepatic lobule (tissue), and the liver (organ).

Concentrations of nutrients and metabolites in the periportal zone (the upper reach of the sinusoid) are inevitably different from those in the perivenous zone (the lower reach) even if the properties of all the hepatocytes are homogeneous, because the downstream hepatocytes accept nutrients and metabolites already taken up and put there by the upstream hepatocytes. Thus a liver model constructed by multiplying single hepatocytes by the number of hepatocytes in the liver would not be representative, but it may be possible to investigate the global behavior of the liver by a simple multiplication of the hepatic lobule, since the liver is a repetitive accumulation of the hepatic lobules as functioning units. Nevertheless, since a human hepatic lobule consists of approximately one million hepatocytes (there are approximately 100 billion hepatocytes and 100,000 lobules in a human liver), simulation of the hepatic lobule at the molecular level is far from realizable with the computational resources currently available. Thereupon, we consider a sinusoid along the porto-central axis (the line between the portal tracts and the central vein) and the surrounding hepatocytes, known as hepatic cords (Figure 1C), to be the primary histological unit for modeling. Since the hepatic lobule has a point symmetry in which the center point is the central vein, the overall behavior of the hepatic lobule and the liver can be derived from that of the porto-central axis. The porto-central axis is the minimal unit preserving the proportionality with the dynamics of the greater, macroscopic structure. Through model construction of the porto-central axis, it becomes possible to investigate the behavior of the liver, at the organ level, based on molecular-level simulations of single hepatocytes.

A multitude of hepatocyte zonal heterogeneities are known [19, 23–25]. Fatty acid oxidation, gluconeogenesis, ureagenesis, amino acid conversion to glucose, cholesterol synthesis, and glutathione peroxidation and conjugation are predominant in the periportal zone; Glycolysis, liponeogenesis, glutamine formation from ammonia, monooxygenation, and glucuronidation are predominant in the perivenous zone. In addition to the heterogeneity generated by the structural constraints described above, enzyme activities regulated by the substrate concentrations in blood, the circulating hormone levels, the autonomic hepatic nerves, and the biomatrix are known to actively modify the conditions of the zonal heterogeneities. Such active regulation of heterogeneities must result from some gain in evolutionary fitness. Since fitness is necessarily the property not of molecules, genes, cells, tissues, or organs, but of classes of organisms [34], the advantage generated by heterogeneous regulation within an organ at the subcellular level must be measured to elucidate the functional activity of the organ that the regulation has evolved. At present, it is extremely hard for the experimental biosciences to measure the properties of an organism simultaneously at multiple levels such as the cell, tissue, and organism. In this study, we constructed a model of the porto-central axis, and obtained insight into the origin of one of the regulated heterogeneities in metabolism, ammonia detoxification.

Ammonia metabolism is one of the most important metabolic pathways for a mammal, since the accumulation of ammonia induces lethal uremia. Ammonia is detoxified exclusively by the hepatocyte in mammals. Accordingly, appropriate ammonia metabolism in the mammalian liver is directly reflected in the health of the organism. The efficiency of ammonia metabolism should therefore link directly with fluctuations of fitness. The fitness fluctuation related to ammonia metabolism may be captured and analyzed through calculation of the efficiency of ammonia detoxification in the porto-central axis unit. The pathway structure of ammonia metabolism around the core of the urea cycle is relatively simple among the major metabolic pathways, and there are a number of biological investigations and several mathematical models for single hepatocytes. The metabolism of ammonia and amino acids is also heterogeneous in the hepatic lobule. The periportal zone is characterized by a high capacity for uptake and catabolism of amino acids (except glutamate and aspartate) as well as for urea synthesis and gluconeogenesis. On the other hand, glutamine synthesis, ornithine transamination, and the uptake of vascular glutamate, aspartate, malate, and α-ketoglutarate are restricted to a small perivenous hepatocyte population [20]. Accordingly, in the hepatic lobule the major pathways for ammonia detoxification and urea and glutamine synthesis are anatomically separated from each other and represent in functional terms the sequence of a periportal low-affinity system (urea synthesis) and a perivenous high-affinity system (glutamine synthesis) for ammonia detoxification [13–18, 20]. Perivenous glutamine synthase-containing hepatocytes act as high-affinity scavengers for the ammonia that escapes the upstream urea-synthesizing compartment.

Three major enzymes involved in ammonia metabolism—carbamoyl phosphate synthase (CPS), ornithine aminotransferase (OAT), and glutamine synthase (GS)—have been characterized as being heterogeneously expressed (synthesized at different rates) in particular locations within the hepatic lobule [5, 9, 10, 22–24]. The regulation of gene expression of these enzymes may be mainly determined not by the substrate concentrations, the hormone levels, or neural regulation, but rather by the histological position of the hepatocyte in the lobule [12, 20, 36, 43, 44]. Additionally, ornithine aminotransferase is demonstrated to be coexpressed with glutamine synthase in perivenous hepatocytes in adult mouse liver, while there is no such coexpression in the kidney, intestine, and brain [30, 31]. One possible explanation of this phenomenon is that the colocalized enzymes lead to more efficient removal of ammonia because ornithine aminotransferase produces glutamate, which is a substrate for glutamine synthase [31]. However, these are still matters of speculation and only subjected to thought experiments. Positional regulation, such as regulation of gene expression, can modulate the pattern of intralobular heterogeneity. Such heterogeneity may appear to be dispensable, but for some reason it is actually present. This raises the question of the purpose for which heterogeneous gene expressions exist. While various possible determinants of the positional regulation of gene expression have been proposed (gradual change in the concentrations

of blood constituents, the extracellular matrix produced by the endothelium of the central venule, intrahepatic cell-cell interaction, etc.), the regulative function of heterogeneous gene expression has been developed evolutionally and has preserved whichever determinants are selected for over time.

Here we show that the positional regulation of gene expression may improve the energy efficiency of ammonia metabolism at the tissue and organ levels, using computer simulation of the porto-central axis unit. Improvement of ammonia detoxification in the liver means increased efficiency at the individual organism level, and this could very well amount to a gain in evolutionary fitness. This suggests that these particular forms of gene expression regulation may reasonably be characterized as advantageous adaptations evolved through natural selection.

2 The Model

We hypothesized that the heterogeneous expression of carbamoyl phosphate synthase, glutamine synthase, and ornithine aminotransferase improves the energy efficiency of ammonia clearance, and therefore increases the evolutionary fitness of the liver, as well as that of the organism. The number of ATP molecules required to eliminate one molecule of ammonia in the hepatic lobule is certainly an appropriate indicator of the energy efficiency of ammonia detoxification. Because ammonia is eliminated by multiple pathways, mainly urea synthesis and glutamine synthesis, the stoichiometry of total ammonia degradation is variable. To calculate the ATP consumption by ammonia metabolism, a simple model of the hepatic lobule was constructed, through a two-step procedure. In the first step, a single-compartment model that consisted of the hepatocyte and the sinusoid, named the *zone model*, was built (Figure 2), and unknown parameters were predicted, as will be described later. In the second step, we modeled the hepatic lobule as a simple compartment model in which eight modeled compartments were connected in series.

The zone model included 67 substances and 29 total reactions consisting of chemical reactions and transportations. Almost all of the known enzymes in the mammalian ammonia metabolism have been described by rate equations. Mathematical models for four enzymes were developed for a urea cycle model developed by Kuchel and his colleagues [29]. Carbamoyl phosphate synthase [7, 8], glutamine synthase [40], phosphate-dependent glutaminase (Glnase) [35, 41], *N*-acetyl glutamate synthetase (AGS) [2, 3], system N (the sodium-dependent glutamine transport system) [32], system L (the sodium-independent glutamine transport system) [32], the ammonia transport system (between the sinusoid and the hepatocellular cytoplasm), the glutamate transport system [11], and the urea transport system (from the hepatocellular cytoplasm to the sinusoid) were modeled using kinetic information obtained from previous publications (see Appendix 1 and Web supplements). The rest of the models, that is, the six enzymes and three transporters, were quoted from a ureagenesis model using a MetaNet graph (see Appendix A1.1) [28]. While MetaNet cannot be guaranteed to reproduce accurate enzyme kinetics [28], it was used with the expectation that it is able to estimate the rates of reactions roughly but sufficiently well.

The metabolite concentrations were determined mainly based on Kohn and his colleagues' work (see Web supplements, Table S1) [28]. The volume ratio of cytoplasm to mitochondria was assumed to be four to one [28], and that between the cytoplasm and the sinusoidal space one to one. Certain kinetic parameters were adjusted under an assumption of steady state. If the model is held in steady state, the following equations are adequately assumed:

$$v_{CPS} = v_{OCT} = v_{OTL} = v_{ASS} = v_{ASL} \tag{1}$$

$$v_{GAMT} = v_{GAT} = v_{ASL} - v_{Argase} \tag{2}$$

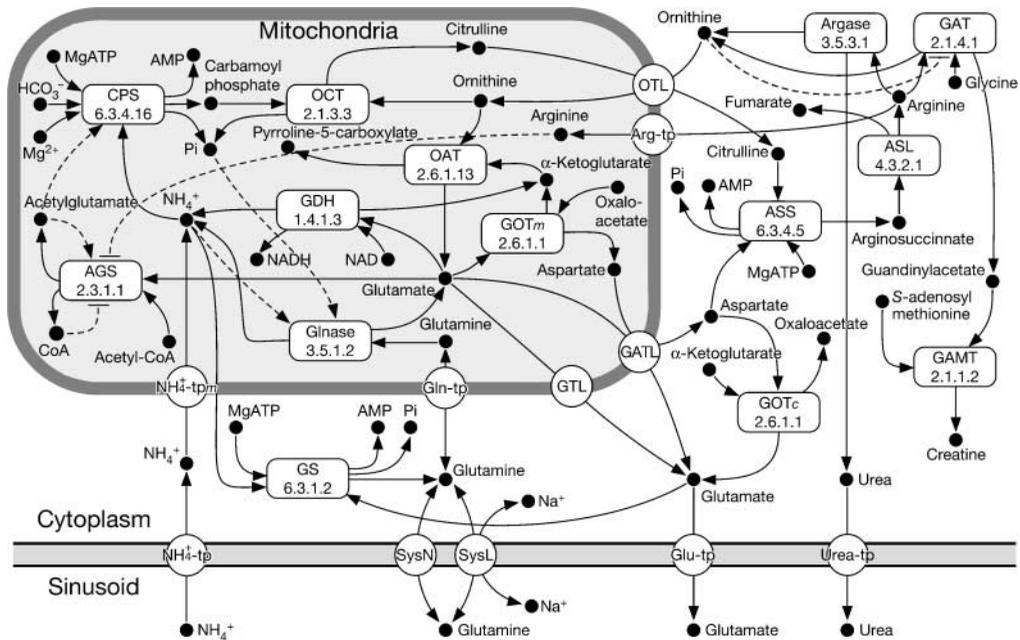$$v_{GOT_m} = v_{GATL} = v_{ASS} = v_{GOT_c} \tag{3}$$

Figure 2. Schematic representation of the model describing ammonia metabolism in single zone model. Filled circles, open rounded rectangles, and open circles represent substances, enzymes, and transporters, respectively. Solid line arrows represent reactions and transportations. Broken lines with a triangular arrowhead and with a bar at one end represent positive and negative feedback, respectively. AGS, *N*-acetyl glutamate synthetase; Argase, arginase; ASL, argininosuccinate lyase; ASS, argininosuccinate synthetase; CPS, carbamoyl phosphate synthetase; GAMT, guanidino-acetate methyltransferase; GAT, arginine:glycine amidinotransferase; GDH, glutamate dehydrogenase; Glnase, phosphate-dependent glutaminase; GOT*c*, glutamate:oxaloacetate transaminase in the cytoplasm; GOT*m*, glutamate:oxaloacetate transaminase in the mitochondria; GS, glutamine synthetase; OAT, ornithine aminotransferase; OCT, ornithine carba-moyltransferase; Arg-tp, arginine transporter; GATL, glutamate-aspartate translocase; Gln-tp, glutamine transporter in mitochondrial membrane; Glu-tp, glutamate transporter; GTL, glutamate translocase; NH_4^+-tp, ammonia transporter in the cell membrane; NH_4^+-tp*m*, ammonia transporter in the mitochondrial membrane; OTL, ornithine-citrulline trans-locase; SysL, system L; SysN, system N; Urea-tp, urea transporter. The entity abbreviation may be used with an index variable that represents the location of the entity. The indices *c*, *m*, and *s* indicate the cytoplasm, mitochondria, and sinusoid, respectively. Numbers in the rounded rectangles represent EC numbers.

Thus, [CPS], [OCT], [OTL], [ASS], [GAMT], [GAT], [GOT$_m$], and [GATL] were determined, based on the premise of [ASL] = 2.2E−6 M [29], v_{Argase} = 6.6E−6 M s^{-1} [29], and [GOT$_c$] = 1E−6 M [28]. The k_{cat}'s of glutaminase and glutamine synthase were calculated from the fluxes through the enzymes in the perfused rat liver: 72 and 151 nmol min^{-1} per gram [19], with the assumptions [GS] = 1E−5 M and [Glnase] = 1E−4 M. The activity of glutaminase was approximated as 1.786E−5 M s^{-1} based on reported conversion factors as follows: 0.8 g hepatocyte wet wt per gram liver wet wt, 0.42 g dry wt per gram hepatocyte wet wt [6], 0.2 ml mitochondrial water per gram dry wt of liver [1]. The activity in M s^{-1} of glutamine synthase was calculated from the ratio of the two enzymes' activities described above. The V_{max}'s of system N and system L were determined from this premise. v_{AGS} and v_{GTL} were set at [AGS] = 2E−5 M [2] and [GTL] = 1E−7 M [28], and $v_{NH_4^+\text{-tp}}$ was assumed to be 5E−5 M s^{-1}. The values of v_{GDH} and v_{OAT} were obtained as follows:

$$v_{\mathrm{GDH}} = v_{\mathrm{CPS}} + v_{\mathrm{GS}} - v_{\mathrm{Glunase}} - v_{NH_4^+\text{-tp}} \tag{4}$$

$$v_{\mathrm{OAT}} = v_{\mathrm{GOT}_m} + v_{\mathrm{GDH}} \tag{5}$$

These equations gave [GDH] and [OAT]. The glutamate transport between the cytoplasm and the sinusoid ($v_{\text{Glu-tp}}$) and the inflow of glutamate from other pathways in mitochondria ($v_{\text{Glu-spp}}$) were modeled to meet the requirements as follows:

$$v_{\text{Glu-tp}} = v_{\text{GS}} + v_{\text{GTL}} - v_{\text{GOT}_c} + v_{\text{GATL}} \tag{6}$$

$$v_{\text{Glu-spp}} = v_{\text{AGS}} - v_{\text{Glunase}} - v_{\text{GTL}} + v_{\text{GOT}_m} + v_{\text{GDH}} - v_{\text{OAT}} - v_{\text{GATL}} \tag{7}$$

In addition, the flux of ornithine from other pathways in mitochondria was set equal to v_{OAT} (see Web supplements, Table S2).

To develop a hepatic lobule model, eight constructed zone models were put in a row and connected one to the next through sinusoidal compartments (Figure 3), in which substances pass through the sinusoids while the hepatocytes are isolated from each other. The first zone (the influx compartment) and the eighth zone (the efflux compartment) were joined to compartments of the upstream periportal tracts and the downstream central vein. Four substances—ammonia, glutamine, glutamate, and urea—flow through the sinusoid and upstream/downstream vessels. Their fluxes from the periportal influx compartment to the perivenous efflux compartment are represented by a simple mass action model as the product of the rate constant and substance concentration (see Appendix 1). No enzymatic reaction is placed in the vessels.

All rate equations and initial concentrations of metabolites were set to be identical among all compartments, but some enzymes were given a slope to their content, representing the regulated heterogeneous gene expressions. In order to evaluate the effects of gradients of the enzyme expressions on metabolic state, six combinations of the gene expression conditions were examined (Table 1). The first model, named the *N model*, had no gradient of the enzyme along the porto-central axis. The second model, named the *GCO model*, in which steep gradients of carbamoyl phosphate synthase, glutamine synthase, and ornithine aminotransferase were introduced, most faithfully modeled the actual lobular ammonia metabolism among the six models. The remaining four models—the *G model*, *GC model*, *O model*, and *GO model*—partially incorporated the enzyme gradients (see Table 1 for details). These significant enzyme slopes were incorporated using a mechanistic model, which assessed the transcription rates of carbamoyl phosphate synthase and glutamine synthase by the relative position in the hepatic lobule (see Appendix A1.3) [5]. In this study, the relative expression levels were assumed to correspond to the transcription rates. The total contents of the enzymes in each model were set equal. The expression status of ornithine aminotransferase was presumed to be evaluable in the same manner as glutamine synthase, based on the reports of coexpression of glutamine synthase and ornithine aminotransferase in the hepatic lobule [30, 31]. Additionally, 60 instances of the models were prepared for each model type by varying the parameters of the flux balance of the glutamate transport system (four patterns): the glutamate flux from outside pathways (three patterns) and the rate constant of sinusoidal substance flow (5 patterns), for a total of $4 \times 3 \times 5 = 60$ patterns (see Appendix A1.4).

3 Methods

3.1 Numerical Integration

Once each chemical and transport reaction rate had been set, a numerical integration of the model was conducted using E-CELL system version 1.1 [42]. The model was implemented by defining the variable Reactor, which describes reaction processes, and the variable Rule, which provides organizational information, substances, and stoichiometry. Simulations were performed using Sun Grid Engine 5.3 on 40 clustered Xeon 2.0 GHz HPC-IAX, and employing the fourth-order Runge-Kutta method. The step interval for integration was set to 0.01 s.
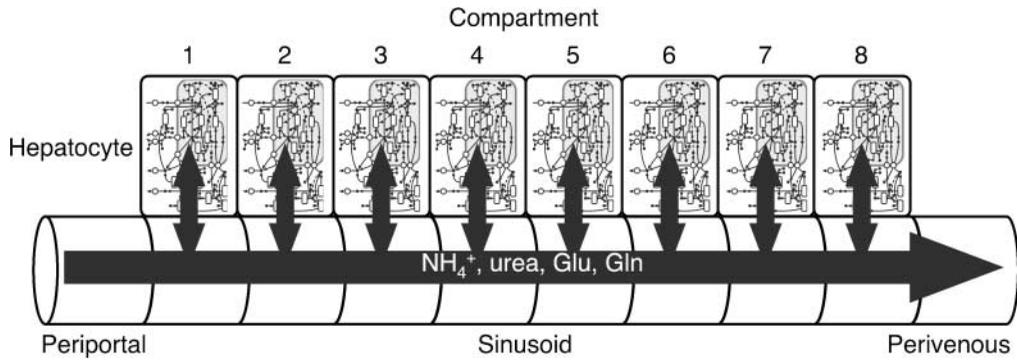
Figure 3. Schematic of eight-cellular-compartment model with sinusoidal compartments. PP and PV represent the periportal end and the perivenous end, respectively. Ammonia (NH_4^+), urea, glutamate (Glu), and glutamine (Gln) flow from the periportal inflow compartment to the perivenous outflow compartment, interacting with cellular compartments.

3.2 Data Analysis

To compare the metabolic aspects in the periportal zone and in the perivenous zone, the flux distributions were examined. To evaluate the effects of the enzyme slope along the lobule metabolic state, the following rates were calculated and used as the indices:

$$\text{Rate of ammonia degradation: } J_{\text{NH}_4^+,\text{deg}} = v_{\text{CPS}} + v_{\text{GS}} \tag{8}$$

$$\text{Rate of ammonia generation: } J_{\text{NH}_4^+,\text{gen}} = v_{\text{Glnase}} + v_{\text{GDH}} \tag{9}$$

$$\text{Rate of ammonia detoxification: } J_{\text{NH}_4^+,\text{detox}} = J_{\text{NH}_4^+,\text{deg}} - J_{\text{NH}_4^+,\text{gen}} \tag{10}$$

$$\text{Rate of ATP consumption: } J_{\text{ATP,consum}} = 2v_{\text{CPS}} + v_{\text{ASS}} \tag{11}$$

Table I. Types of model. Six models examined in this study had different combinations of enzyme gradients along the porto-central axis. Letters G, C, and O included in the names of model types are the first letter of gradually expressed enzymes: glutamine synthase (GS), carbamoyl phosphate synthase (CS), and ornithine aminotransferase (OAT), respectively. Enzyme gradients were incorporated into models in an all-or-none fashion. Symbol + or − means whether the enzyme gradient existed in the models. The letters G, C, and O also indicate the existence of the gradient of the respective enzyme. The N model had no gradient of the enzyme.

	Gradual expression of enzyme		
Model type	GS	CPS	OAT
N	−	−	−
G	+	−	−
GC	+	+	−
O	−	−	+
GO	+	−	+
GCO	+	+	+

Energy efficiency $\eta := \dfrac{J_{\mathrm{NH_4^+,detox}}}{J_{\mathrm{ATP,consum}}}$ (12)

Rate of bicarbonate consumption $: J_{\mathrm{HCO_3^-,consum}} = v_{\mathrm{CPS}}$ (13)

$R_{\mathrm{NH_4^+,detox}}$ and $v_{\mathrm{NH_4^+\text{-}tp}}$ are nearly equal under the assumption of steady state. Data were summarized as the mean $\pm$ SD of 60 models for each gradient pattern of the model.

4 Results

4.1 Simulation of the Single-Zone Model
The zone model, which consists of a hepatocellular compartment and a sinusoidal compartment, preserved a quasi steady state for longer than 100,000 s with the initial values mainly quoted from the published literature based on experimental data (see Web supplement, Table S1). The results support the appropriateness of the zone model, as described below.

4.2 Comparison of the Hepatic Lobule Models with Different Enzyme Expressions Patterns
Each model with slopes of the various enzyme expressions exhibits lobule-wide metabolic aspects very different from the N model with no such enzymatic slope. The simulated flux heterogeneities among the porto-central axis are presented in Figures 4 and 5. In the GCO model, which is the best-approximated model to actual lobular metabolism, the active pathways were quite different between the periportal and the perivenous zones (Figure 4). Urea production, urea exportation, and creatine generation were pronouncedly predominant in the periportal zone (red arrows in Figure 4B, Figure 5F a, b, j, k, l, q, t), while glutamine formation and exportation were predominantly seen in the perivenous zone (blue arrows in Figure 4B, Figure 5F c, d, e, h, i, o, r, s). Because mitochondrial ornithine aminotransferase is mainly expressed in the perivenous zone, the concentration of glutamate, which is a reaction product of ornithine aminotransferase, was higher in the perivenous than in the periportal zone. The glutamate concentration in mitochondria was increased from $6.97\mathrm{E}{-3}$ to $8.70\mathrm{E}{-2}$ M along the porto-central axis. Consequently, the velocity of glutamate dehydrogenase, which catalyzes glutamate, was larger in the perivenous than in the periportal zone (Figure 5F d). Glutamate-aspartate translocase and mitochondrial GOT also exhibited higher activities in the perivenous zone, while cytoplasmic GOT showed an opposite trend of flux between the periportal and the perivenous zone (Figure 4B, Figure 5F e, i, o). Cytoplasmic GOT catalyzed transamination between glutamate and oxaloacetate to produce aspartate, and the generated bulk of aspartate was used as a substrate for argininosuccinate synthetase in the periportal zone (Figure 4B, Figure 5F j). In the N model with no enzyme gradient, most of the chemical reactions and transportation exhibited larger fluxes in the periportal zone than in the perivenous zone (Figure 5A). Due to the high affinity for ammonia of glutamine synthetase, namely, 1/10 of the K_m of carbamoyl phosphate synthetase, ammonia predominantly converted to glutamine in the periportal zone. The fluxes gently changed from the periportal to the perivenous zone, while dramatic alterations were seen in the sixth and seventh compartments in the GCO model, revealing that the perivenous hepatocytes played a lesser role in metabolism in the N model (Figure 5A, F). The G model and the GC model exhibited higher activities of ureagenesis in the periportal zone and greater formation and export of glutamine in the perivenous zone, just like the GCO model. However, in contrast to the GCO model, larger fluxes of OAT, GDH, mitochondrial GOT, and GATL were observed in both models (Figure 5B,C c, d, e, o). In the O model, most of the reactions exhibited higher activity in the perivenous zone, except for the predominant detoxification of ammonia by glutamine synthetase (Figure 5D). Lobule-wide metabolic aspects of the GO model resembled those of the GCO model except for the urea cycle and glutamate transport (Figure 5E). There were fewer contrasts in activities of the urea
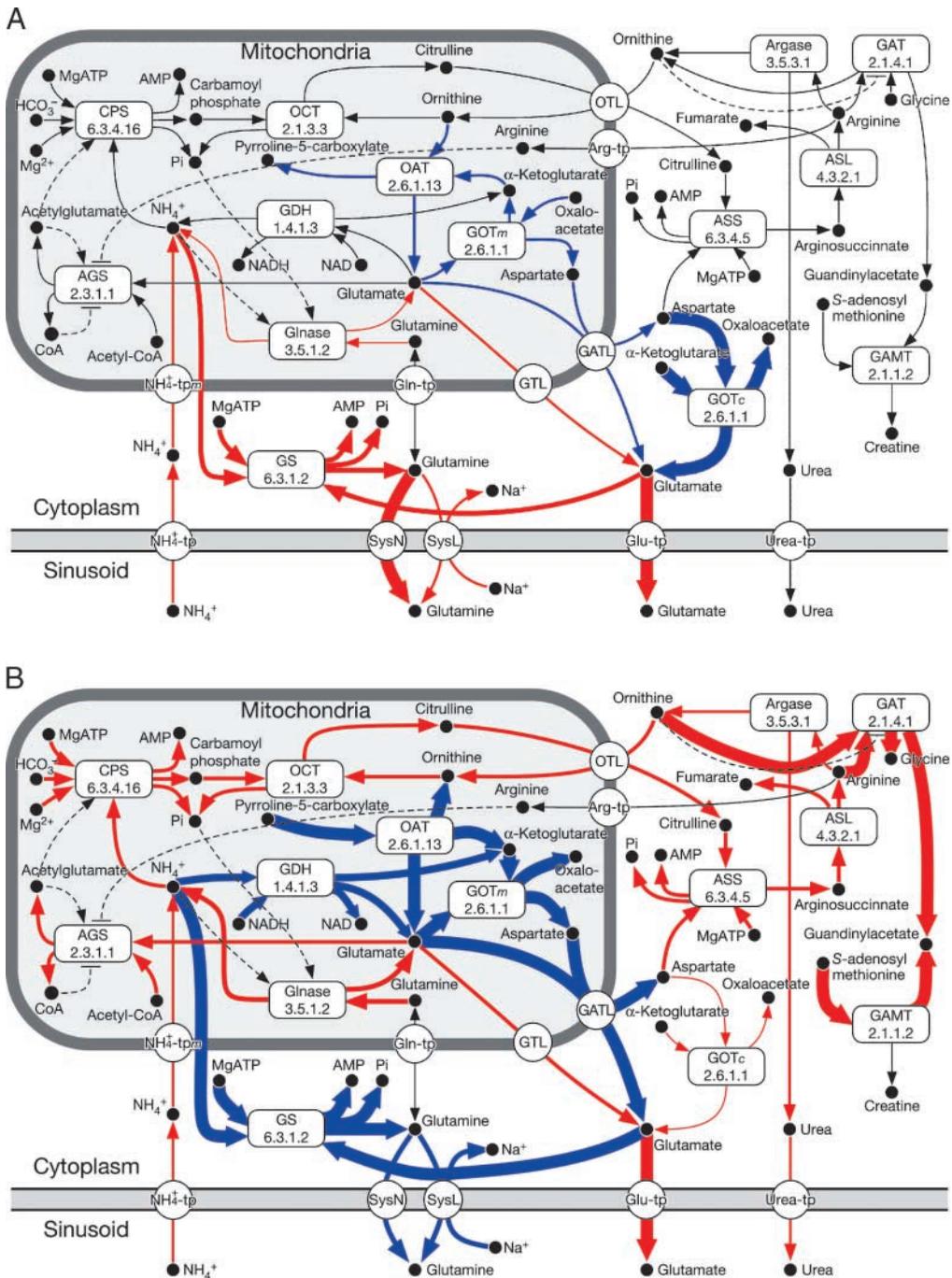
Figure 4. Flux disparities between the two ends of the porto-central axis in N model (A) and GCO model (B). The width of each arrow proportionally reflects the flux ratio between the two ends (the first and the eighth compartment). The thickest line indicates the flux disparity to be fivefold or more. Red and blue arrows indicate fluxes predominant in the periportal and the perivenous zone, respectively. Fluxes with a disparity of less than 1.5 are indicated by the black arrow. The size of the arrows is proportional to the flux except for extremely high fluxes: the Glu-tp in A, ornithine amino-transferase, mitochondrial GOT, and GATL in B. Pronounced urea production, urea export, and creatine generation were seen in the periportal region, while pronounced glutamine formation and reactions which mediate glutamate were seen in the perivenous. The figure shows a representative result among the 60 parameter conditions (see Appendix A1.4 for details).
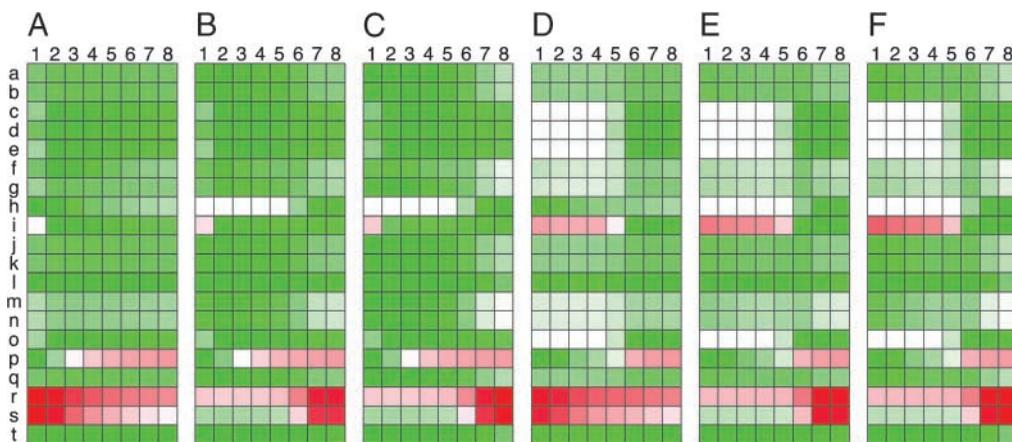
Figure 5. Flux heterogeneities along the porto-central axis. Relative fluxes of 20 representative processes (enzyme reaction or transportation across a membrane) are indicated as color matrices. For each process, the depth of color is proportional to the relative magnitude of its flux, and the maximum absolute flux is indicated by the deepest color. Green and red indicate positive and negative direction of the process, respectively. Colors within the same process are comparable, but inter-process comparison is inappropriate. The numbers on the horizontal axis (1–8) indicate the compartment number. Therefore, the left side represents the periportal and the right side represents the perivenous zone. Panel A, N model; B, G model; C, GC model; D, O model; E, GO model; F, GCO model. On the vertical axis: a, CPS; b, OCT; c, OAT; d, GDH; e, GOT$_m$; f, Glnase; g, AGS; h, GS; i, GOT$_c$; j, ASS; k, ASL; l, Argase; m, GAT; n, GAMT; o, GATL; p, GTL; q, OTL; r, SysL; s, SysN; t, Urea-tp. The figure shows a representative result among the 60 parameter conditions (see Appendix A1.4 for details).

cycle and glutamate transport along the porto-central axis in the GO model than in the GCO model (Figure 5E).

4.3 Evaluation of the Effects of Gene Expression Gradients along the Porto-central Axis

The GCO model ranks highest among six models in the rate and energy efficiency of ammonia detoxification. The mean rate of elimination of ammonia from the sinusoid was 11.8% greater in the GCO model than in the control (N model) (Table 2). Although the rate of degradation of ammonia in all eight compartments was 20.0% slower in the GCO model than in the control, the rate of ammonia generation was also 53.8% slower than in the control model (Table 2), showing that the GCO model was able to remove ammonia more efficiently than the control. The mean rate of ATP consumption in the GCO model was 9.5% less than in the control model (Table 2). The O model and GO model also exhibited less ATP consumption than the control. The energy efficiency η, which means the number of consumed ATP molecules required for the elimination of one ammonia molecule, was smaller in the GCO model than in the control (Figure 5, 3.59 $\pm$ 0.22 versus 4.47 $\pm$ 0.49). The O model and the GO model also displayed smaller η, and the G model and the GC model greater η, than the control (Figure 6).

Elimination of bicarbonate in the GCO model was comparable in rate to that in the control (Table 2). The G and GC models exhibited greater elimination of bicarbonate, but the O and GO models exhibited a lesser elimination of bicarbonate, than the control (Table 2).

5 Discussion

In this study, a mathematical model in which rough histological structure and several forms of regulation of gene expression has been implemented, and it succeeded in representing the metabolic heterogeneity of ammonia detoxification in the liver. Heterogeneous flux distributions bearing a close resemblance to the actual hepatic lobule were observed along the porto-central axis in the

Table 2. The rates of metabolic processes of five models relative to the N model. The highest relative rate of ammonia detoxification was seen in the GCO model. The O model had the lowest relative rate of ATP consumption and the lowest relative rate of bicarbonate consumption.

Process	Relative rate					
	Model N	G	GC	O	GO	GCO
Ammonia degradation	1.00	0.95	1.01	0.79	0.76	0.80
Ammonia generation	1.00	1.00	0.99	0.48	0.46	0.46
Ammonia detoxification	1.00	0.90	1.03	1.09	1.04	1.12
ATP consumption	1.00	1.12	1.19	0.78	0.86	0.90
Bicarbonate consumption	1.00	1.26	1.34	0.77	0.94	0.99

GCO model, which is an approximation of the actual regulation of gene expression in the ammonia-metabolism-related enzymes. The periportal hepatocytes play a role in urea production and creatine generation, while the perivenous cells play a role in glutamine generation and glutamate metabolism in this model (Figure 4). The model without any regulation of gene expression, the N model, also displayed heterogeneous metabolism, but the extent of the heterogeneity was quite reduced compared to the GCO model, indicating that two factors, the histological structure and gradual gene expression, are likely sufficient to simulate the zonal heterogeneity in liver ammonia detoxification, while the histological structure alone was insufficient. The simulation results also suggest that the gradients of expression of the three enzymes (CPS, GS, and OAT) along the porto-central axis improve the energy efficiency of ammonia detoxification (Table 2 and Figure 6).

Flux distributions in the model with the gradients of CPS, GS, and OAT are close to the schemes of heterogeneous ammonia metabolism in the lobule discussed in many reports [20, 31]. It has been suggested that urea production and bicarbonate consumption in exchange for ammonia detoxification by the urea cycle are more highly activated in periportal hepatocytes, and glutamine generation and reactions that mediate glutamate (OAT, GDH) are more highly activated in perivenous (opposite-side) hepatocytes [20, 31]. Three enzymes, CPS, GS, and OAT, chiefly restrict and characterize the flux distributions in each zone. The flux distributions between the periportal and perivenous zone have a mutually exclusive relationship. Glutamine metabolism (both of synthesis and consumption) was
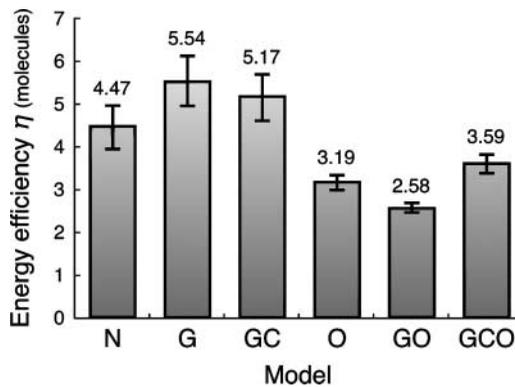

Figure 6. Energy efficiency in the six models with different gene expression patterns. Energy efficiencies η were calculated from $J_{NH_4^+,detox}$ and $J_{ATP,consum}$ (see text for details). Data are means $\pm$ SD.

hardly seen in the periportal zone, while urea production and creatine generation were not seen in the perivenous zone. Cytoplasmic GOT showed opposite trends between the two zones. Ornithine aminotransferase in the perivenous hepatocytes is speculated to lead to an accumulation of glutamate, which is the substrate for glutamine synthetase, and to increase the elimination of ammonia [31].

Our model differs in some features from previous investigations. Glutamate dehydrogenase has been suggested to have significantly increased activity in the perivenous zone [33]. In our model, higher activities were also shown in the perivenous than in the periportal zone, but the direction of the reaction was different from the suggestion in a previous report [4]. For glutamate dehydrogenase in the perivenous zone, a reverse reaction to that suggested by other investigators was predominant [4]. This might be attributable to the lack of the α-ketoglutarate transport system in our model. If that mechanism were implemented in our model and the influxes of α-ketoglutarate to the perivenous mitochondria increased, the reaction direction might be the same as suggested by previous work. Phosphate-dependent glutaminase has been suggested to be highly activated in the periportal zone [20, 45]. However, the tendency towards emphasized activity of phosphate-dependent glutaminase in the periportal hepatocytes was not recreated in our model.

Several factors are considered to be responsible for the result in our experiments. One factor is the roughness of the mathematical model of phosphate-dependent glutaminase, such as the lack of a pH effect despite the actual high sensitivity to pH [41]. Another factor is the absence of regulation of phosphate-dependent glutaminase gene expression. It might be necessary to give a slope to gene expression along the hepatic lobule, as we did with GS, OAT, and CPS. Although this model does not yet have the requisite accuracy, it is the first realization of a model able to yield metabolic aspects with both quantitative information at the micro, or kinetic, level and functional significance at the macro, or tissue, level in the liver.

It is proposed that one major advantage of the functional separation in the hepatic lobule is that the periportal urea synthesis flux is flexible with regard to the requirement of the acid-base condition without the risk of hyperammonemia, because effective elimination of ammonia is carried out by perivenous glutamine synthetase [13−18, 20]. It is also proposed that ornithine aminotransferase, which is co-localized with glutamine synthetase, would lead to more efficient removal of ammonia. In this study, because the effect of pH is excluded, no indication is given of its relation to the major advantage of the functional separation, which has been discussed by previous investigators. But it is newly suggested that the functional separation that is formed by steep gradients of GS, OAT, and CPS along the hepatic lobule contributes to effective ammonia elimination with efficient energy use. Interestingly, the glutamine synthetase and ornithine aminotransferase expression patterns are not the same in other organs, such as the kidney, brain, and intestine [31]. This fact indicates cooperation of the expression of the two enzymes evolved specifically in the hepatic lobule. The steep gradients of the three enzymes along the porto-central axis are considered to have been evolved into effective ammonia detoxification, which takes place exclusively in the liver. Although the improvement in the energy efficiency shown by simulation is not robust, it is sufficient to confer an adaptive advantage, since ammonia metabolism consumes a large quantity of ATP in the liver. Schneider and colleagues have reported ureagenesis accounts for 15% of the total energy consumption of rat hepatocytes incubated in a nutriment-enriched medium [38]. Ultimately, this simulation will have to be verified with wet (physiological) experiments, but it is difficult to evaluate changes in the lobular energy efficiency along with changes in the porto-central axial regulation of gene expression by wet experiments at present. Technology is continually advancing, however, and the day should not be far off when such confirmation will be within reach.

In summary, we have shown that a novel systems biological approach for tissue modeling well simulated the functional separation in the hepatic lobule, and the simulation results suggested contribution of the gradual expressions of three enzyme (CPS, GS, and OAT) along the porto-central axis to effective ammonia detoxification with efficient energy use. This method of reconstructing the intracellular chemical processes, based on module architectures such as the hepatic lobule, enables analysis of certain metabolic aspects with both quantitative information at the kinetic level and functional significance at the tissue level, and to evaluate the effect of enzyme gene expression gradients on metabolic

state. We here present a novel model system constructed by merging the single-cell model, which consisted of intracellular biochemical reactions, together with a proper structure (the histological structure of the hepatic lobule) and emergent new properties of a higher-level order (zonal heterogeneity in ammonia metabolism). Using such a model, it is possible to study how nanoscopic and microscopic biological entities influence mesoscopic and macroscopic biological phenomena. Such approaches hold great promise for advancing our understanding of complicated multicellular tissues, organs, and the organism in a fitness landscape. This is an extremely useful and exclusive feature of systems biology.

Acknowledgments

References

1. Achs, M. J., Anderson, J. H., & Garfinkel, D. (1971). Gluconeogenesis in rat liver cytosol. I. Computer analysis of experimental data. *Computers and Biomedical Research, an International Journal, 4*(1), 65–106.

2. Bachmann, C., & Colombo, J. P. (1981). Computer simulation of the urea cycle: Trials for an appropriate model. *Enzyme, 26*(5), 259–264.

3. Bachmann, C., Krahenbuhl, S., & Colombo, J. P. (1982). Purification and properties of acetyl-CoA:L-glutamate *n*-acetyltransferase from human liver. *The Biochemical Journal, 205*(1), 123–127.

4. Boon, L., Geerts, W. J., Jonker, A., Lamers, W. H., & Van Noorden, C. J. (1999). High protein diet induces pericentral glutamate dehydrogenase and ornithine aminotransferase to provide sufficient glutamate for pericentral detoxification of ammonia in rat liver lobules. *Histochemistry and Cell Biology, 111*(6), 445–452.

5. Christoffels, V. M., Sassi, H., Ruijter, J. M., Moorman, A. F., Grange, T., & Lamers, W. H. (1999). A mechanistic model for the development and maintenance of portocentral gradients in gene expression in the liver. *Hepatology, 29*(4), 1180–1192.

6. Crawford, J. M., & Blum, J. J. (1983). Quantitative analysis of flux along the gluconeogenic, glycolytic and pentose phosphate pathways under reducing conditions in hepatocytes isolated from fed rats. *The Biochemical Journal, 212*(3), 585–598.

7. Elliott, K. R., & Tipton, K. F. (1974). Kinetic studies of bovine liver carbamoyl phosphate synthetase. *The Biochemical Journal, 141*(3), 807–816.

8. Elliott, K. R., & Tipton, K. F. (1974). Product inhibition studies on bovine liver carbamoyl phosphate synthetase. *The Biochemical Journal, 141*(3), 817–824.

9. Gebhardt, R. (1992). Metabolic zonation of the liver: Regulation and implications for liver function. *Pharmacology & Therapeutics, 53*(3), 275–354.

10. Gebhardt, R., Gaunitz, F., & Mecke, D. (1994). Heterogeneous (positional) expression of hepatic glutamine synthetase: Features, regulation and implications for hepatocarcinogenesis. In G. Weber & C. E. Forrest Weber (Eds.), *Advances in enzyme regulation: Proceedings of the Twenty-Seventh Symposium on Regulation of Enzyme Activity and Synthesis in Normal and Neoplastic TI* (pp. 3427–3456). New York: Elsevier Science.

11. Gebhardt, R., & Mecke, D. (1983). Glutamate uptake by cultured rat hepatocytes is mediated by hormonally inducible, sodium-dependent transport systems. *FEBS Letters, 161*(2), 275–278.

12. Gupta, S., Rajvanshi, P., Sokhi, R. P., Vaidya, S., Irani, A. N., & Gorla, G. R. (1999). Position-specific gene expression in the liver lobule is directed by the microenvironment and not by the previous cell differentiation state. *The Journal of Biological Chemistry, 274*(4), 2157–2165.

13. Haussinger, D. (1989). Glutamine metabolism in the liver: Overview and current concepts. *Metabolism: Clinical and Experimental, 38*(8 Suppl. 1), 14–17.

14. Haussinger, D. (1990). Nitrogen metabolism in liver: Structural and functional organization and physiological relevance. *The Biochemical Journal, 267*(2), 281–290.

15. Haussinger, D. (1990). Organization of hepatic nitrogen metabolism and its relation to acid-base homeostasis. *Klinische Wochenschrift*, *68*(22), 1096−1101.

16. Haussinger, D. (1992). Liver and systemic pH-regulation. *Zeitschrift für Gastroenterologie*, *30*(2), 147−150.

17. Haussinger, D. (1997). Liver regulation of acid-base balance. *Mineral and Electrolyte Metabolism*, *23*(3−6), 249−252.

18. Haussinger, D. (1998). Hepatic glutamine transport and metabolism. *Advances in Enzymology and Related Areas of Molecular Biology*, *72*, 43−86.

19. Haussinger, D., Gerok, W., & Sies, H. (1983). Regulation of flux through glutaminase and glutamine synthetase in isolated perfused rat liver. *Biochimica et Biophysica Acta*, *755*(2), 272−278.

20. Haussinger, D., Lamers, W. H., & Moorman, A. F. (1992). Hepatocyte heterogeneity in the metabolism of amino acids and ammonia. *Enzyme*, *46*(1−3), 72−93.

21. Ideker, T., Galitski, T., & Hood, L. (2001). A new approach to decoding life: Systems biology. *Annual Review of Genomics and Human Genetics*, *2*, 343−372.

22. Jungermann, K. (1986). Functional heterogeneity of periportal and perivenous hepatocytes. *Enzyme*, *35*(3), 161−180.

23. Jungermann, K. (1995). Zonation of metabolism and gene expression in liver. *Histochemistry and Cell Biology*, *103*(2), 81−91.

24. Jungermann, K., & Katz, N. (1989). Functional specialization of different hepatocyte populations. *Physiological Reviews*, *69*(3), 708−764.

25. Jungermann, K., & Kietzmann, T. (1996). Zonation of parenchymal and nonparenchymal metabolism in liver. *Annual Review of Nutrition*, *16*, 179−203.

26. Kitano, H. (2002). Systems biology: A brief overview. *Science*, *295*(5560), 1662−1664.

27. Kohn, M. C. (1992). Propagation of information in metanet graph models. *Journal of Theoretical Biology*, *154*(4), 505−517.

28. Kohn, M. C., Tohmaz, A. S., Giroux, K. J., Blumenthal, G. M., Feezor, M. D., & Millington, D. S. (2002). Robustness of metanet graph models: Predicting control of urea production in humans. *Bio Systems*, *65*(1), 61−78.

29. Kuchel, P. W., Roberts, D. V., & Nichol, L. W. (1977). The simulation of the urea cycle: Correlation of effects due to inborn errors in the catalytic properties of the enzymes with clinical-biochemical observations. *The Australian Journal of Experimental Biology and Medical Science*, *55*(3), 309−326.

30. Kuo, F. C., & Darnell, J. E., Jr. (1991). Evidence that interaction of hepatocytes with the collecting (hepatic) veins triggers position-specific transcription of the glutamine synthetase and ornithine aminotransferase genes in the mouse liver. *Molecular and Cellular Biology*, *11*(12), 6050−6058.

31. Kuo, F. C., Hwu, W. L., Valle, D., & Darnell, J. E. (1991). Colocalization in pericentral hepatocytes in adult mice and similarity in developmental expression pattern of ornithine aminotransferase and glutamine synthetase mRNA. *Proceedings of the National Academy of Sciences of the United States of America*, *88*(21), 9468−9472.

32. Low, S. Y., Salter, M., Knowles, R. G., Pogson, C. I., & Rennie, M. J. (1993). A quantitative analysis of the control of glutamine catabolism in rat liver cells. Use of selective inhibitors. *The Biochemical Journal*, *295*(Pt. 2), 617−624.

33. Maly, I. P., & Sasse, D. (1991). Microquantitative analysis of the intra-acinar profiles of glutamate dehydrogenase in rat liver. *The Journal of Histochemistry and Cytochemistry*, *39*(8), 1121−1124.

34. Maynard Smith, J. (1998). *Evolutionary genetics*, (2nd ed.) New York: Oxford University Press.

35. McGivan, J. D., & Bradford, N. M. (1983). Characteristics of the activation of glutaminase by ammonia in sonicated rat liver mitochondria. *Biochimica et Biophysica Acta*, *759*(3), 296−302.

36. Notenboom, R. G., de Boer, P. A., Moorman, A. F., & Lamers, W. H. (1996). The establishment of the hepatic architecture is a prerequisite for the development of a lobular pattern of gene expression. *Development*, *122*(1), 321−332.

37. Sasse, D., Spornitz, U. M., & Maly, I. P. (1992). Liver architecture. *Enzyme*, *46*(1−3), 8−32.

38. Schneider, W., Siems, W., & Grune, T. (1990). Balancing of energy-consuming processes of rat hepatocytes. *Cell Biochemistry and Function*, 8(4), 227–232.

39. Segel, I. H. (1993). *Enzyme kinetics: Behavior and analysis of rapid equilibrium and steady state enzyme systems.* New York: Wiley.

40. Seyama, S., Kuroda, Y., & Katunuma, N. (1972). Purification and comparison of glutamine synthetase from rat and chick livers. *Journal of Biochemistry*, 72(4), 1017–1027.

41. Szweda, L. I., & Atkinson, D. E. (1989). Response of rat liver glutaminase to pH. Mediation by phosphate and ammonium ions. *The Journal of Biological Chemistry*, 264(26), 15357–15360.

42. Tomita, M., Hashimoto, K., Takahashi, K., Shimizu, T. S., Matsuzaki, Y., Miyoshi, F., Saito, K., Tanida, S., Yugi, K., Venter, J. C., & Hutchison, C. A., III. (1999). E-CELL: Software environment for whole-cell simulation. *Bioinformatics*, 15(1), 72–84.

43. Wagenaar, G. T., Chamuleau, R. A., de Haan, J. G., Maas, M. A., de Boer, P. A., Marx, F., Moorman, A. F., Frederiks, W. M., & Lamers, W. H. (1993). Experimental evidence that the physiological position of the liver within the circulation is not a major determinant of zonation of gene expression. *Hepatology*, 18(5), 1144–1153.

44. Wagenaar, G. T., Chamuleau, R. A., Maas, M. A., de Bruin, K., Korfage, H. A., & Lamers, W. H. (1994). The physiological position of the liver in the circulation is not a major determinant of its functional capacity. *Hepatology*, 20(6), 1532–1540.

45. Watford, M. (1993). Hepatic glutaminase expression: Relationship to kidney-type glutaminase and to the urea cycle. *The FASEB Journal*, 7(15), 1468–1474.

Appendix 1: Details of Mathematical Model

A1.1 Mathematical Models of Chemical Reactions and Transports
See Web Supplement, Table S3, for parameter values.

A1.1.1 Carbamoyl Phosphate Synthetase (EC. 6.3.4.16)
The enzyme catalyzes

$$2ATP + NH_4^+ + HCO_3^- \rightarrow 2AMP + 2Pi + CP$$
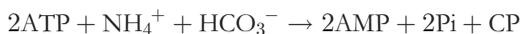
in mitochondria. The kinetic model was obtained from previous literature [7, 8]:

$$v_{CPS} = \frac{k_{cat,CPS}[CPS]}{\text{denominator}_{CPS}}$$

where

$$\text{denominator}_{\text{CPS}} = 1 + \frac{K_{\text{mATP}_1,\text{CPS}} + K_{\text{mATP}_2,\text{CPS}}}{[\text{ATP}]} + \frac{K_{\text{mHCO}_3^-,\text{CPS}}}{\left[\text{HCO}_3^-\right]} + \frac{K_{\text{mNAG},\text{CPS}}}{[\text{NAG}]} + \frac{K_{\text{mNH}_4^+,\text{CPS}}}{\left[\text{NH}_4^+\right]}$$

$$+ \frac{K_{\text{sATP}_1,\text{CPS}}K_{\text{m'HCO}_3^-,\text{CPS}} + K_{\text{sHCO}_3^-,\text{CPS}}\left(K_{\text{mATP}_2,\text{CPS}} + K_{\text{m'ATP}_2,\text{CPS}}\right)}{[\text{ATP}]} + \frac{K_{\text{sNAG},\text{CPS}}K_{\text{mATP}_1,\text{CPS}}}{[\text{ATP}][\text{NAG}]}$$

$$+ \frac{K_{\text{sMg}^{2+},\text{CPS}}K_{\text{mATP}_1,\text{CPS}}}{[\text{ATP}]\left[\text{Mg}^{2+}\right]} + \frac{K_{\text{sATP}_2,\text{CPS}}K_{\text{mNH}_4^+,\text{CPS}}}{[\text{ATP}]\left[\text{NH}_4^+\right]} + \frac{K_{\text{sNAG},\text{CPS}}K_{\text{m'HCO}_3^-,\text{CPS}}}{[\text{NAG}]\left[\text{HCO}_3^-\right]}$$

$$+ \frac{K_{\text{sNAG},\text{CPS}}K_{\text{sMg}^{2+},\text{CPS}}K_{\text{mATP}_1,\text{CPS}}}{[\text{ATP}]\left[\text{Mg}^{2+}\right][\text{NAG}]}$$

$$+ \frac{K_{\text{sATP}_1,\text{CPS}}K_{\text{sNAG},\text{CPS}}K_{\text{m'HCO}_3^-,\text{CPS}} + K_{\text{sNAG},\text{CPS}}K_{\text{sHCO}_3^-,\text{CPS}}K_{\text{m'ATP}_2,\text{CPS}}}{[\text{ATP}][\text{NAG}]\left[\text{HCO}_3^-\right]}$$

$$+ \frac{K_{\text{sATP}_1,\text{CPS}}K_{\text{sMg}^{2+},\text{CPS}}K_{\text{m'HCO}_3^-,\text{CPS}}}{[\text{ATP}]\left[\text{Mg}^{2+}\right]\left[\text{HCO}_3^-\right]} + \frac{K_{\text{sATP}_2,\text{CPS}}K_{\text{sHCO}_3^-,\text{CPS}}K_{\text{m'HCO}_3^-,\text{CPS}}\left(K_{\text{mNH}_4^+,\text{CPS}} + K_{\text{m'NH}_4^+,\text{CPS}}\right)}{[\text{ATP}]\left[\text{HCO}_3^-\right]\left[\text{NH}_4^+\right]}$$

$$+ \frac{K_{\text{sATP}_1,\text{CPS}}K_{\text{sMg}^{2+},\text{CPS}}K_{\text{sNAG},\text{CPS}}K_{\text{m'HCO}_3^-,\text{CPS}}}{[\text{ATP}]\left[\text{Mg}^{2+}\right][\text{NAG}]\left[\text{HCO}_3^-\right]} + \frac{K_{\text{sATP}_2,\text{CPS}}K_{\text{sNAG},\text{CPS}}K_{\text{sHCO}_3^-,\text{CPS}}K_{\text{m'NH}_4^-,\text{CPS}}}{[\text{ATP}][\text{NAG}]\left[\text{HCO}_3^-\right]\left[\text{NH}_4^+\right]}$$

$$+ \frac{K_{\text{sATP}_1,\text{CPS}}K_{\text{sHCO}_3^-,\text{CPS}}K_{\text{m'ATP}_2,\text{CPS}}}{[\text{ATP}]^2\left[\text{HCO}_3^-\right]} + \frac{K_{\text{sATP}_1,\text{CPS}}K_{\text{sNAG},\text{CPS}}K_{\text{sHCO}_3^-,\text{CPS}}K_{\text{m'ATP}_2,\text{CPS}}}{[\text{ATP}]^2[\text{NAG}]\left[\text{HCO}_3^-\right]}$$

$$+ \frac{K_{\text{sATP}_1,\text{CPS}}K_{\text{sMg}^{2+},\text{CPS}}K_{\text{sHCO}_3^-,\text{CPS}}K_{\text{m'ATP}_2,\text{CPS}}}{[\text{ATP}]^2\left[\text{Mg}^{2+}\right]\left[\text{HCO}_3^-\right]} + \frac{K_{\text{sATP}_1,\text{CPS}}K_{\text{sATP}_2,\text{CPS}}K_{\text{sHCO}_3^-,\text{CPS}}K_{\text{m'NH}_4^+,\text{CPS}}}{[\text{ATP}]^2\left[\text{HCO}_3^-\right]\left[\text{NH}_4^+\right]}$$

$$+ \frac{K_{\text{sATP}_1,\text{CPS}}K_{\text{sMg}^{2+},\text{CPS}}K_{\text{sNAG},\text{CPS}}K_{\text{sHCO}_3^-,\text{CPS}}K_{\text{m'ATP}_2,\text{CPS}}}{[\text{ATP}]^2\left[\text{Mg}^{2+}\right][\text{NAG}]\left[\text{HCO}_3^-\right]}$$

$$+ \frac{K_{\text{sATP}_1,\text{CPS}}K_{\text{sATP}_2,\text{CPS}}K_{\text{sMg}^{2+},\text{CPS}}K_{\text{sHCO}_3^-,\text{CPS}}K_{\text{m'NH}_4^+,\text{CPS}}}{[\text{ATP}]^2\left[\text{Mg}^{2+}\right]\left[\text{HCO}_3^-\right]\left[\text{NH}_4^+\right]}$$

$$+ \frac{K_{\text{sATP}_1,\text{CPS}}K_{\text{sATP}_2,\text{CPS}}K_{\text{sNAG},\text{CPS}}K_{\text{sHCO}_3^-,\text{CPS}}K_{\text{m'NH}_4^+,\text{CPS}}}{[\text{ATP}]^2[\text{NAG}]\left[\text{HCO}_3^-\right]\left[\text{NH}_4^+\right]}$$

$$+ \frac{K_{\text{sATP}_1,\text{CPS}}K_{\text{sATP}_2,\text{CPS}}K_{\text{sMg}^{2+},\text{CPS}}K_{\text{sNAG},\text{CPS}}K_{\text{sHCO}_3^-,\text{CPS}}K_{\text{m'NH}_4^+,\text{CPS}}}{[\text{ATP}]^2\left[\text{Mg}^{2+}\right][\text{NAG}]\left[\text{HCO}_3^-\right]\left[\text{NH}_4^+\right]}$$

A1.1.2 N-Acetyl Glutamate Synthetase (EC. 2.3.1.1)

The enzymes catalyze AcCoA + Glu → CoA + NAG.

The reaction mechanism is a nonreversible rapid equilibrium random bi-bi mechanism [3]:

$$v_{\mathrm{AGS}} = \frac{\dfrac{k_{\mathrm{cat,AGS}}[\mathrm{AGS}][\mathrm{AcCoA}][\mathrm{Glu}]}{\left(1 + \dfrac{K_{\mathrm{aArg,AGS}}}{[\mathrm{Arg}]}\right)}}{\mathrm{denominator_{AGS}}}$$

where

$$\begin{aligned}
\mathrm{denominator_{AGS}} &= K_{\mathrm{iAcCoA,AGS}} K_{\mathrm{mGlu,AGS}} \left(1 + \frac{[\mathrm{CoA}]}{K_{\mathrm{iCoA,AGS}}}\right)\left(1 + \frac{[\mathrm{NAG}]}{K_{\mathrm{iNAG,AGS}}}\right) \\
&\quad + K_{\mathrm{mGlu,AGS}}\left(1 + \frac{[\mathrm{NAG}]}{K_{\mathrm{iNAG,AGS}}}\right)[\mathrm{AcCoA}] \\
&\quad + K_{\mathrm{mAcCoA,AGS}}\left(1 + \frac{[\mathrm{CoA}]}{K_{\mathrm{iCoA,AGS}}}\right)[\mathrm{Glu}] + [\mathrm{AcCoA}][\mathrm{Glu}]
\end{aligned}$$

A1.1.3 Glutamine Synthetase (EC. 6.3.1.2)

The enzyme catalyzes ATP + Glu + $\mathrm{NH_4^+}$ → AMP + Pi + Gln:

$$v_{\mathrm{GS}} = \frac{k_{\mathrm{cat,GS}}[\mathrm{GS}][\mathrm{Glu}][\mathrm{ATP}][\mathrm{NH_4^+}]}{\left(K_{\mathrm{mGlu,GS}} + [\mathrm{Glu}]\right)\left(K_{\mathrm{mATP,GS}} + [\mathrm{ATP}]\right)\left(K_{\mathrm{mNH_4^+,GS}} + [\mathrm{NH_4^+}]\right)}$$

A1.1.4 Phosphate-Dependent Glutaminase (EC. 3.5.1.2)

The enzyme catalyzes Gln + Pi → Glu + $\mathrm{NH_4^+}$. It is activated by the product: ammonia [27]. Co-operativity of glutamine and Pi, which is an essential activator for phosphate-dependent glutaminase, were modeled by the Hill equation [39]:

$$v_{\mathrm{Glnase}} = \frac{\dfrac{k_{\mathrm{cat,Glnase}}[\mathrm{Glnase}]}{1 + \dfrac{K_{\mathrm{a,Glnase}}}{\left[\mathrm{NH_4^+}\right]}}[\mathrm{Gln}]^{n_{\mathrm{Gln,Glnase}}}}{[\mathrm{Gln}]_{0.5}^{n_{\mathrm{Gln,Glnase}}}\left(1 + \dfrac{[\mathrm{Pi}]_{0.5}^{n_{\mathrm{Pi,Glnase}}}}{[\mathrm{Pi}]^{n_{\mathrm{Pi,Glnase}}}}\right) + [\mathrm{Gln}]^{n_{\mathrm{Gln,Glnase}}}\left(1 + \dfrac{[\mathrm{Pi}]_{0.5}^{n_{\mathrm{Pi,Glnase}}}}{[\mathrm{Pi}]^{n_{\mathrm{Pi,Glnase}}}}\right)}$$

A1.1.5 Ornithine Carbamoyltransferase (EC. 2.1.3.3)

The enzyme catalyzes CP + Orn ↔ Pi + Cit. The reaction mechanism is an ordered bi-bi sequential mechanism [29]:

$$
v_{\text{OCT}} = \frac{\left(k_{1,\text{OCT}}k_{3,\text{OCT}}k_{5,\text{OCT}}k_{7,\text{OCT}}[\text{CP}][\text{Orn}] - k_{2,\text{OCT}}k_{4,\text{OCT}}k_{6,\text{OCT}}k_{8,\text{OCT}}[\text{Cit}][\text{Pi}]\right)[\text{OCT}]}{\text{denominator}_{\text{OCT}}}
$$

where

$$
\begin{aligned}
\text{denominator}_{\text{OCT}} = {} & k_{2,\text{OCT}}k_{7,\text{OCT}}\left(k_{4,\text{OCT}} + k_{5,\text{OCT}}\right) + k_{1,\text{OCT}}k_{7,\text{OCT}}\left(k_{4,\text{OCT}} + k_{5,\text{OCT}}\right)[\text{CP}] \\
& + k_{2,\text{OCT}}k_{8,\text{OCT}}\left(k_{4,\text{OCT}} + k_{5,\text{OCT}}\right)[\text{Pi}] + k_{3,\text{OCT}}k_{5,\text{OCT}}k_{7,\text{OCT}}[\text{Orn}] \\
& + k_{2,\text{OCT}}k_{4,\text{OCT}}k_{6,\text{OCT}}[\text{Cit}] + k_{1,\text{OCT}}k_{3,\text{OCT}}\left(k_{5,\text{OCT}} + k_{7,\text{OCT}}\right)[\text{CP}][\text{Orn}] \\
& + k_{6,\text{OCT}}k_{8,\text{OCT}}\left(k_{2,\text{OCT}} + k_{4,\text{OCT}}\right)[\text{Pi}][\text{Cit}] + k_{1,\text{OCT}}k_{4,\text{OCT}}k_{6,\text{OCT}}[\text{CP}][\text{Cit}] \\
& + k_{1,\text{OCT}}k_{3,\text{OCT}}k_{6,\text{OCT}}[\text{CP}][\text{Orn}][\text{Cit}] + k_{3,\text{OCT}}k_{5,\text{OCT}}k_{8,\text{OCT}}[\text{Orn}][\text{Pi}] \\
& + k_{3,\text{OCT}}k_{6,\text{OCT}}k_{8,\text{OCT}}[\text{Orn}][\text{Pi}][\text{Cit}]
\end{aligned}
$$

A1.1.6 Argininosuccinate Synthetase (EC. 6.3.4.5)

The enzyme catalyzes ATP + Cit + Asp ↔ AMP + Pi + ASA. The reaction mechanism is an ordered ter-ter mechanism [29]:

$$
v_{\text{ASS}} = \frac{\left(k_{1,\text{ASS}}k_{3,\text{ASS}}k_{5,\text{ASS}}k_{7,\text{ASS}}k_{9,\text{ASS}}k_{11,\text{ASS}}[\text{Cit}][\text{Asp}][\text{ATP}] - k_{2,\text{ASS}}k_{4,\text{ASS}}k_{6,\text{ASS}}k_{8,\text{ASS}}k_{10,\text{ASS}}k_{12,\text{ASS}}[\text{ASA}][\text{AMP}][\text{Pi}]\right)}{\text{denominator}_{\text{ASS}}}[\text{ASS}]
$$

where

$$
\begin{aligned}
\text{denominator}_{\text{ASS}} = {} & k_{2,\text{ASS}}k_{4,\text{ASS}}k_{9,\text{ASS}}k_{11,\text{ASS}}\left(k_{6,\text{ASS}}+k_{7,\text{ASS}}\right) \\
& + k_{1,\text{ASS}}k_{4,\text{ASS}}k_{6,\text{ASS}}k_{8,\text{ASS}}k_{11,\text{ASS}}[\text{Cit}][\text{Pi}] \\
& + k_{1,\text{ASS}}k_{4,\text{ASS}}k_{9,\text{ASS}}k_{11,\text{ASS}}\left(k_{6,\text{ASS}}+k_{7,\text{ASS}}\right)[\text{Cit}] \\
& + k_{2,\text{ASS}}k_{5,\text{ASS}}k_{7,\text{ASS}}k_{9,\text{ASS}}k_{12,\text{ASS}}[\text{Asp}][\text{ASA}] \\
& + k_{2,\text{ASS}}k_{5,\text{ASS}}k_{7,\text{ASS}}k_{9,\text{ASS}}k_{11,\text{ASS}}[\text{Asp}] \\
& + k_{1,\text{ASS}}k_{3,\text{ASS}}k_{6,\text{ASS}}k_{8,\text{ASS}}k_{11,\text{ASS}}[\text{Cit}][\text{ATP}][\text{Pi}] \\
& + k_{1,\text{ASS}}k_{3,\text{ASS}}k_{9,\text{ASS}}k_{11,\text{ASS}}\left(k_{6,\text{ASS}}+k_{7,\text{ASS}}\right)[\text{Cit}][\text{ATP}] \\
& + k_{1,\text{ASS}}k_{4,\text{ASS}}k_{6,\text{ASS}}k_{8,\text{ASS}}k_{10,\text{ASS}}[\text{Cit}][\text{AMP}][\text{Pi}] \\
& + k_{1,\text{ASS}}k_{5,\text{ASS}}k_{7,\text{ASS}}k_{9,\text{ASS}}k_{11,\text{ASS}}[\text{Cit}][\text{Asp}] \\
& + k_{3,\text{ASS}}k_{5,\text{ASS}}k_{7,\text{ASS}}k_{9,\text{ASS}}k_{12,\text{ASS}}[\text{ATP}][\text{Asp}][\text{ASA}] \\
& + k_{3,\text{ASS}}k_{5,\text{ASS}}k_{7,\text{ASS}}k_{9,\text{ASS}}k_{11,\text{ASS}}[\text{ATP}][\text{Asp}] \\
& + k_{2,\text{ASS}}k_{5,\text{ASS}}k_{7,\text{ASS}}k_{9,\text{ASS}}k_{12,\text{ASS}}[\text{AMP}][\text{Asp}][\text{ASA}] \\
& + k_{2,\text{ASS}}k_{4,\text{ASS}}k_{9,\text{ASS}}k_{12,\text{ASS}}\left(k_{6,\text{ASS}}+k_{7,\text{ASS}}\right)[\text{ASA}] \\
& + k_{1,\text{ASS}}k_{3,\text{ASS}}k_{6,\text{ASS}}k_{8,\text{ASS}}k_{10,\text{ASS}}[\text{Cit}][\text{ATP}][\text{AMP}][\text{Pi}] \\
& + k_{1,\text{ASS}}k_{3,\text{ASS}}k_{5,\text{ASS}}\left(k_{7,\text{ASS}}k_{9,\text{ASS}}+k_{7,\text{ASS}}k_{11,\text{ASS}}+k_{9,\text{ASS}}k_{11,\text{ASS}}\right)[\text{Cit}][\text{ATP}][\text{Asp}] \\
& + k_{1,\text{ASS}}k_{3,\text{ASS}}k_{5,\text{ASS}}k_{8,\text{ASS}}k_{11,\text{ASS}}[\text{Cit}][\text{Asp}][\text{ATP}][\text{Pi}] \\
& + k_{2,\text{ASS}}k_{4,\text{ASS}}k_{6,\text{ASS}}k_{8,\text{ASS}}k_{11,\text{ASS}}[\text{Pi}] \\
& + k_{1,\text{ASS}}k_{3,\text{ASS}}k_{5,\text{ASS}}k_{7,\text{ASS}}k_{10,\text{ASS}}[\text{Cit}][\text{Asp}][\text{ATP}][\text{AMP}] \\
& + k_{2,\text{ASS}}k_{4,\text{ASS}}k_{6,\text{ASS}}k_{8,\text{ASS}}k_{10,\text{ASS}}[\text{AMP}][\text{Pi}] \\
& + k_{3,\text{ASS}}k_{5,\text{ASS}}k_{7,\text{ASS}}k_{10,\text{ASS}}k_{12,\text{ASS}}[\text{Asp}][\text{ATP}][\text{ASA}][\text{AMP}] \\
& + k_{2,\text{ASS}}k_{4,\text{ASS}}k_{6,\text{ASS}}k_{8,\text{ASS}}k_{12,\text{ASS}}[\text{ASA}][\text{Pi}]
\end{aligned}
$$

A1.1.7 Argininosuccinate Lyase (EC. 4.3.2.1)

The enzyme catalyzes ASA $\leftrightarrow$ Fum + Arg. The reaction mechanism is an ordered uni-bi mechanism:

$$v_{\text{ASL}} = \frac{\left(k_{1,\text{ASL}}k_{3,\text{ASL}}k_{5,\text{ASL}}[\text{ASA}] - k_{2,\text{ASL}}k_{4,\text{ASL}}k_{6,\text{ASL}}[\text{Fum}][\text{Arg}]\right)[\text{ASL}]}{\begin{array}{l} k_{5,\text{ASL}}\left(k_{2,\text{ASL}} + k_{3,\text{ASL}}\right) + k_{1,\text{ASL}}\left(k_{3,\text{ASL}} + k_{5,\text{ASL}}\right)[\text{ASA}] + k_{2,\text{ASL}}k_{4,\text{ASL}}[\text{Fum}] \\ + k_{6,\text{ASL}}\left(k_{2,\text{ASL}} + k_{3,\text{ASL}}\right) + k_{4,\text{ASL}}k_{6,\text{ASL}}[\text{Fum}][\text{Arg}] + k_{1,\text{ASL}}k_{4,\text{ASL}}[\text{ASA}][\text{Fum}] \end{array}}$$
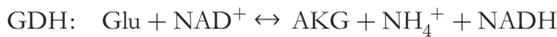
A1.1.8 Arginase (EC. 3.5.3.1)

The enzyme catalyzes Arg $\rightarrow$ urea + Orn. The reaction is an irreversible process and inhibited by ornithine:

$$v_{\text{Argase}} = \frac{k_{1,\text{Argase}}k_{3,\text{Argase}}k_{4,\text{Argase}}[\text{Arn}][\text{Argase}]}{\begin{array}{l} k_{4,\text{Argase}}\left(k_{2,\text{Argase}} + k_{3,\text{Argase}}\right) + k_{5,\text{Argase}}\left(k_{2,\text{Argase}} + k_{3,\text{Argase}}\right)[\text{Orn}] \\ + k_{1,\text{Argase}}\left(k_{3,\text{Argase}} + k_{4,\text{Argase}}\right)[\text{Arn}] \end{array}}$$

A1.1.9 MetaNet Model

OTL, GTL, GATL, OAT, GOT_m, GOT_c, GDH, GAT, and GAMT were modeled using MetaNet [28]. The reaction stoichiometries were defined as follows:

OTL: $\text{Cit}_m + \text{Orn}_c \leftrightarrow \text{Cit}_c + \text{Orn}_m$

GTL: $\text{Glu}_c \leftrightarrow \text{Glu}_m$

GATL: $\text{Glu}_c + \text{Asp}_m \leftrightarrow \text{Glu}_m + \text{Asp}_c$

OAT: $\text{Orn} + \text{AKG} \leftrightarrow \text{Pyrroline-5-carboxylate} + \text{Glu}$

GOT_m: $\text{Glu} + \text{OAA} \leftrightarrow \text{Asp} + \text{AKG}$

GOT_c: $\text{Asp} + \text{AKG} \leftrightarrow \text{Glu} + \text{OAA}$

GDH: $\text{Glu} + \text{NAD}^+ \leftrightarrow \text{AKG} + \text{NH}_4^+ + \text{NADH}$

GAT: $\text{Gly} + \text{Arg} \leftrightarrow \text{Orn} + \text{GAA}$

GAMT: $\text{SAM} + \text{GAA} \rightarrow \text{Cre}$

Although MetaNet is not guaranteed to accurately reproduce enzyme kinetics, it was used in our model with the expectation it would roughly estimate the rates of reactions. The velocities of the reactions were calculated as follows:

$$v_x = \frac{V_{\max,x}\left(1 - \frac{V_{r,x}}{V_{f,x}}\frac{\prod\limits_{j_x}\left(\frac{c_{j_x}}{K'_{j_x,x}}\right)}{\prod\limits_{i_x}\left(\frac{c_{i_x}}{K'_{i_x,x}}\right)}\right)}{1 + \sum\limits_{i_x}\left(\frac{c_{i_x}}{K'_{i_x,x}}\right)^{n_{i_x,x}}\left(1 + \sum\limits_{j_x}\left(\frac{c_{j_x}}{K'_{j_x,x}}\right)^{n_{j_x,x}}\right)\left(1 + \sum\limits_{k'_x}\left(\frac{K'_{k_x,x}}{c_{k'_x}}\right)^{n_{k'_x,x}} + \sum\limits_{b'_x}\left(\frac{c_{b'_x}}{K'_{b_x,x}}\right)^{n_{b'_x,x}}\right)}$$

where

$$K'_{s,x} = K_{s,x} \left(1 + \sum_{k_x} \left(\frac{K_{k_x,x}}{c_{k_x}} \right)^{n_{k_x,x}} + \sum_{h} \left(\frac{c_{h_x}}{K_{h,x,x}} \right)^{n_{h_x,x}} \right)$$

$K_{s,x}$ and $n_{s,x}$ are the binding constant and the *cooperativity index* (essentially a Hill exponent) of substance (or effector) s of enzyme x (equilibrium constant for dissociation of the enzyme-ligand complex), respectively, and $K'_{s,x}$ is the former's effective binding constant, which reflects the activities of the competitive activators k_x and the competitive inhibitors h_x; c_s is the concentration of substance s; and k'_x and h'_x are the noncompetitive activators and noncompetitive inhibitors of the reaction catalyzed by enzyme x, respectively [27].

A1.1.10 System N
Glutamine is transported into the cytoplasm by a sodium-dependent transport mechanism. This process is inhibited by histidine [32]:

$$v_{\text{SysN}} = V_{\text{max,SysN}} \left[\left(\frac{[\text{Na}^+]_e}{[\text{Na}^+]_e + K_{\text{mNa,SysN}}} \right) \left(\frac{[\text{Glu}]_e}{[\text{Glu}]_e + K_{\text{mGlu,SysN}} \left(1 + \frac{[\text{His}]_e}{K_{\text{iHis,SysN}}} \right)} \right) \right.$$

$$\left. - \left(\frac{[\text{Na}^+]_c}{[\text{Na}^+]_c + K_{\text{mNa,SysN}}} \right) \left(\frac{[\text{Glu}]_c}{[\text{Glu}]_c + K_{\text{mGlu,SysN}} \left(1 + \frac{[\text{His}]_c}{K_{\text{iHis,SysN}}} \right)} \right) \right]$$

A1.1.11 System L
Glutamine is transported into the cytoplasm by a sodium-independent transport mechanism. This process is inhibited by tryptophan [32].

$$v_{\text{SysL}} = V_{\text{max,SysL}} \left(\frac{[\text{Glu}]_e}{[\text{Glu}]_e + K_{\text{mGlu,SysL}} \left(1 + \frac{[\text{Trp}]_e}{K_{\text{iTrp,SysL}}} \right)} - \frac{[\text{Glu}]_c}{[\text{Glu}]_c + K_{\text{mGlu,SysL}} \left(1 + \frac{[\text{Trp}]_c}{K_{\text{iTrp,SysL}}} \right)} \right)$$

A1.1.12 Ammonia Transport between Sinusoid and Cytoplasm
Ammonia transport between the sinusoid and cytoplasm was modeled based on the general mass action law:

$$v_{\text{NH}_4^+4\text{-tp}} = k_{\text{NH}_4^+4\text{-tp}} \left(\left[\text{NH}_4^+ \right]_c - \left[\text{NH}_4^+ \right]_e \right)$$

A1.1.13 Transportation of Glutamine, Arginine, and Ammonia between Cytoplasm and Mitochondria
Transports of glutamine, arginine, and ammonia across the mitochondrial membrane were presumed to rapidly attain equilibrium:

$$K_{\text{eq},x} \left([\text{S}]_c - v_x \right) = \left([\text{S}]_m + v_x \right)$$

A1.1.14 Urea Transport to Sinusoid

Excretion of urea in the sinusoidal space was modeled based on the general mass action law:

$$v_{\text{Urea-tp}} = k_{\text{Urea-tp}}\big([\text{urea}]_c - [\text{urea}]_e\big)$$

A1.1.15 Glutamate Transport between Sinusoid and Cytoplasm

Glutamate transport between the sinusoid and cytoplasm was modeled as Michaelis-Menten reversible kinetics:

$$v_{\text{Glu-tp}} = V_{mF,\text{Glu-tp}}\left(\frac{[\text{Glu}]_e}{[\text{Glu}]_e + K_{m\text{Glu},\text{Glu-tp}}}\right) - V_{mR,\text{Glu-tp}}\left(\frac{[\text{Glu}]_c}{[\text{Glu}]_c + K_{m\text{Glu},\text{Glu-tp}}}\right)$$

A1.1.16 Glutamate Flux from the Outside Pathways

Glutamate flux from the outside pathways of the model was represented by the difference between zero-order influx and efflux based on the general mass action law:

$$v_{\text{Glu-spp}} = J_{\text{Glu-spp}} - k_{\text{Glu-spp}}[\text{Glu}]_c$$

A1.1.17 Degradation of Metabolites

Degradation of N-acetyl glutamate, Pi, and CoA was modeled based on the general mass action law under the assumption of steady state:

$$v_{\text{deg},s} = k_{\text{deg},s}[s]$$

where s is a substance.

A1.1.18 Ornithine Inflow from Other Reactions

To hold the steady state, ornithine inflow from other reactions was presumed to be equal to the flux of ornithine aminotransferase, v_{OAT}.

A1.2 Mathematical Model of Metabolite Flows in Sinusoid

Flows of ammonia, glutamine, glutamate, and urea from the nth sinusoidal compartment to the n+1th compartment, v_{e,s_n}, were modeled based on the general mass action law:

$$v_{e,s_n} = k_e[s_n]_e$$

where s_n represents a substance in the nth compartment of the sinusoid.

A1.3 Mathematical Model of Gene Expression of Carbamoyl Phosphate Synthetase, Glutamine Synthetase, and Ornithine Aminotransferase in Hepatic Lobule

To describe the regulated gene expression of three enzymes—carbamoyl phosphate synthetase, glutamine synthetase, and ornithine aminotransferase—along the porto-central axis, we adopted the

mechanistic model proposed by Christoffels et al. [5]. The model is based on simple receptor-ligand kinetics, and the parameters are fitted by experimental values. [F_x^*] is the concentration of the active transcription factor F of enzyme x, and assumed as follows [5]:

Carbamoyl phosphate synthetase: $[F_{CPS}^*] = 0.2 - 0.01X$

Glutamine synthetase and ornithine aminotransferase: $[F_{GS}^*] = [F_{OAT}^*] = 0.1X$

where X is the radius of the hepatic lobule: $X = 0$ corresponds to the portal tracts, and $X = 10$ corresponds to the central vein. Thus, X was defined as follows in our model:

$$X = 10 \times \frac{n}{\text{total number of sinusoidal compartments}}$$

where n is the number of a compartment among the eight compartments, $n = 1$ corresponds to the compartment adjacent to the portal tracts, and $n = 8$ corresponds to the compartment adjacent to the central vein. The total number of sinusoidal compartments is eight in our model.

$R_{GX,x}$ is the relative rate of transcription, assumed to correspond to the transcription rate in our model. $R_{GX,x}$ is calculated using the fractional saturation $Y_{GX,x}$, the dissociation constant $K_{GX,x}$, and the Hill coefficient $n_{GX,x}$ as follows [5]:

$$Y_{GX,x} = \frac{[F_x^*]^{n_{GX,x}}}{[F_x^*]^{n_{GX,x}} + K_{GX,x}{}^{n_{GX,x}}}$$

$$R_{GX,x} = R_{max,GX,x} Y_{GX,x}$$

Carbamoyl phosphate synthetase was fitted with high-affinity ($Y_{GX,CPS,h}$) and low-affinity ($Y_{GX,CPS,l}$) units as follow [5]:

$$R_{GX,CPS} = R_{max,GX,CPS} \left(Y_{GX,CPS,h} + Y_{GX,CPS,l} \right)$$

A1.4 Varying the Uncertain Parameters

The rate constants for glutamate supply from other pathways (the glutamate transport system and the sinusoidal flow model) were uncertain. Therefore we prepared 60 model instances for each type by varying these rate constant values under a steady-state assumption.

Figures 4 and 5 presented the results under the conditions in Table 3 as a representative of the 60 model instances in each gene expression pattern; after 50,000 s from the start of simulation, with the value $3E-5$ M s^{-1} for the glutamate influx from pathways outside of the model, the ratio of $V_{mF,\text{Glu-tp}}$ and $V_{mR,\text{Glu-tp}}$ were set to 4.15 in the glutamate transport system, and $k_e = 1.0$ in the sinusoidal flow model.

Appendix 2: Abbreviations

CPS, carbamoyl phosphate synthetase; GS, glutamine synthetase; OAT, ornithine aminotransferase; AGS, N-acetyl glutamate synthetase; Glnase, phosphate-dependent glutaminase; OCT, ornithine carbamoyltransferase; ASS, argininosuccinate synthetase; ASL, argininosuccinate lyase; Argase, arginase;

Table 3. Variation parameters.

___

Regulation of gene expression

1. Not incorporated (N model)

2. Incorporated GS, CPS, and OAT gradients (GCO model)

3. Incorporated only GS gradients (G model)

4. Incorporated GS and CPS gradients (GC model)

5. Incorporated OAT gradients (O model)

6. Incorporated GS and OAT gradients (GO model)

Glutamate transporter

1. $V_{mF,\text{Glu-tp}} : V_{mR,\text{Glu-tp}} = 4.15$ ($V_{mF,\text{Glu-tp}} = 1.0629\text{E}{-}2$ M s^{-1}, $V_{mR,\text{Glu-tp}} = 2.5611\text{E}{-}3$ M s^{-1})

2. $V_{mF,\text{Glu-tp}} : V_{mR,\text{Glu-tp}} = 4.5$ ($V_{mF,\text{Glu-tp}} = 1.2573\text{E}{-}3$ M s^{-1}, $V_{mR,\text{Glu-tp}} = 2.7940\text{E}{-}4$ M s^{-1})

3. $V_{mF,\text{Glu-tp}} : V_{mR,\text{Glu-tp}} = 5.0$ ($V_{mF,\text{Glu-tp}} = 6.1467\text{E}{-}4$ M s^{-1}, $V_{mR,\text{Glu-tp}} = 1.2293\text{E}{-}4$ M s^{-1})

4. $V_{mF,\text{Glu-tp}} : V_{mR,\text{Glu-tp}} = 7.0$ ($V_{mF,\text{Glu-tp}} = 2.6560\text{E}{-}4$ M s^{-1}, $V_{mR,\text{Glu-tp}} = 3.7943\text{E}{-}5$ M s^{-1})

Glutamate Flux from Outside Pathways

1. $J_{\text{Glu-spp}} = 3\text{E}{-}5$ M s^{-1}, $k_{\text{Glu-spp}} = 7.0866\text{E}{-}2$ s^{-1}

2. $J_{\text{Glu-spp}} = 6\text{E}{-}5$ M s^{-1}, $k_{\text{Glu-spp}} = 8.2539\text{E}{-}2$ s^{-1}

3. $J_{\text{Glu-spp}} = 8\text{E}{-}5$ M s^{-1}, $k_{\text{Glu-spp}} = 9.0321\text{E}{-}2$ s^{-1}

Substance Flow in Sinusoid

1. $k_e = 0.5$

2. $k_e = 0.8$

3. $k_e = 1.0$

4. $k_e = 1.2$

5. $k_e = 1.6$

___

GOT, glutamate:oxaloacetate; GDH, glutamate dehydrogenase; GAT, arginine:glycine amidinotransferase; GAMT, guanidinoacetate methyltransferase; OTL, ornithine-citrulline translocase; GTL, glutamate translocase; GATL, glutamate-aspartate translocase; NH_4^+-tp, ammonia transporter; Glu-tp, glutamate transporter; Gln-tp, glutamine transporter in mitochondrial membrane; Urea-tp, urea transporter. The entity abbreviation may be used with an index that represents the location of the entity. The indices c, m, and s indicate the cytoplasm, mitochondria, and sinusoid, respectively.